Polariton assisted incoherent to coherent excitation energy transfer between colloidal nanocrystal quantum dots

Kaiyue Peng[1, a)] and Eran Rabani[1, 2, 3, b)]
[1)] *Department of Chemistry, University of California, Berkeley, California 94720, United States*
[2)] *Materials Sciences Division, Lawrence Berkeley National Laboratory, Berkeley, California 94720, United States*
[3)] *The Sackler Center for Computational Molecular and Materials Science, Tel Aviv University, Tel Aviv 69978, Israel*

(Dated: June 17, 2024)

We explore the dynamics of energy transfer between two nanocrystal quantum dots placed within an optical microcavity. By adjusting the coupling strength between the cavity photon mode and the quantum dots, we have the capacity to fine-tune the effective coupling between the donor and acceptor. Introducing a non-adiabatic parameter, γ, governed by the coupling to the cavity mode, we demonstrate the system's capability to shift from the overdamped Förster regime ($\gamma \ll 1$) to an underdamped coherent regime ($\gamma \gg 1$). In the latter regime, characterized by swift energy transfer rates, the dynamics are influenced by decoherence times. To illustrate this, we study the exciton energy transfer dynamics between two closely positioned CdSe/CdS core/shell quantum dots with sizes and separations relevant to experimental conditions. Employing an atomistic approach, we calculate the excitonic level arrangement, exciton–phonon interactions, and transition dipole moments of the quantum dots within the microcavity. These parameters are then utilized to define a model Hamiltonian. Subsequently, we apply a generalized non-Markovian quantum Redfield equation to delineate the dynamics within the polaritonic framework.

Keywords: Quantum Dots, Polariton, Micro–cavity, Coherent energy transfer

I. INTRODUCTION

In the realm of nanophotonics and quantum optics, understanding and controlling the transfer of energy between quantum emitters is paramount for advancing technologies ranging from solar cells to quantum information processing.[1–3] Colloidal nanocrystal (NC) quantum dots (QDs), with unique electronic and optical properties,[4–6] have emerged as versatile platforms for studying energy transfer processes at the nanoscale.[1,7–9] Among these processes, Fluorescence Resonance Energy Transfer (FRET) has garnered considerable attention for its role in mediating efficient energy transfer between quantum dots[1,9,10] and other emitters[11,12] and has been extensively studied and exploited in various fields, including molecular biology,[13,14] where it serves as a fundamental tool for probing molecular interactions and dynamics.[12,15,16] FRET, an incoherent energy transfer process,[17,18] relies on the weak coupling between a donor and an acceptor fluorophore, with a transfer rate given by Fermi's golden rule (FGR):[19,20]

$$k_{\mathrm{FGR}} = \frac{2\pi}{\hbar} \sum_{\mathcal{DA}} \rho_{\mathcal{D}} \left| J_{\mathcal{DA}} \right|^2 \delta \left(E_{\mathcal{D}} - E_{\mathcal{A}} \right). \qquad (1)$$

Here, $\rho_{\mathcal{D}}$ is the population distribution of excited states on the donor, $J_{\mathcal{DA}}$ is the electromagnetic coupling between transition densities connecting the ground state and excited state for the donor and the acceptor (approximated by the dipole-dipole term, see Eq. (3) below), and $E_{\mathcal{D}}$ and $E_{\mathcal{A}}$ are the donor and acceptor excited state energies, respectively. When the emission spectrum of the donor overlaps with the absorption spectrum of the acceptor and they are within a certain distance, typically within a few nanometers, energy transfer can occur with high efficiency, but on relatively long timescales (a few tens of nanoseconds).[10,11,20–23] FRET processes are inherently limited by the steep distance dependence (R^{-3}) of the dipole-dipole coupling between the donor and acceptor QDs, resulting in small couplings, overdamped energy transfer dynamics, and long transfer rates, necessitating the exploration of alternative mechanisms to accelerate and control the energy transfer mechanism.[24–26]

One strategy for regulating the exciton energy transfer process involves utilizing a donor-bridge-acceptor configuration, wherein the transition mechanism and rates can be adjusted by manipulating the states of the bridge.[27,28] Recent advancements have led to the emergence of polariton–mediated energy transfer as a promising alternative to FRET.[25,29,30] Polaritons, arising from the strong coupling between photons and excitons, present distinct advantages for facilitating energy transfer, such as heightened coupling strength and diminished sensitivity to spectral overlap.[25,26,30–32] As efforts intensify to exploit polariton-mediated energy transfer, ongoing research endeavors are dedicated to elucidating the control parameters dictating the efficiency and dynamics of these processes.[24,26,33,34]

In this study, we examine the dynamics of energy transfer between two quantum dots (QDs) situated in an op-

[a)] Electronic mail: kaiyue_peng@berkeley.edu
[b)] Electronic mail: eran.rabani@berkeley.edu

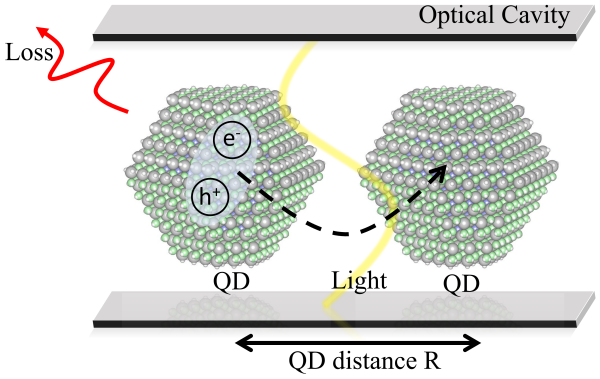

Figure 1. An illustration of two core/shell quantum dots in an optical microcavity.

tical microcavity, as depicted in Fig. 1. By adjusting the coupling strength between the cavity photon mode and the QDs, we can manipulate the effective coupling between the donor and acceptor while maintaining the system reorganization energy almost constant. We demonstrate that this ability to control the effective coupling between the donor and acceptor, without altering other aspects of the system, offers a means to transition the system from the overdamped Förster regime to an underdamped coherent regime, where the transfer rate is influenced by decoherence time.

To illustrate this transition to coherent energy transfer dynamics, we examine two closely positioned CdSe/CdS core/shell QDs of sizes and separations relevant to experimental conditions. We utilize an atomistic theory to compute the excitonic level structure,[35,36] exciton–phonon couplings,[36,37] and transition dipole moments of the two QDs within a microcavity setting. To capture the intricate interplay among photons, phonons, and excitons, we employ a generalized non-Markovian quantum Redfield equation, which provides a framework for accurately describing both populations and coherences under weak exciton–phonon coupling conditions, suitable for CdSe and CdS materials. We employ a non-adiabatic parameter, γ, influenced by the coupling to the cavity mode (among other factors) and demonstrate that in the nonadiabatic regime ($\gamma \ll 1$), our approach aligns with Förster theory without the necessity of specifying the spectral line width, as it is self-determined by the Redfield approach. As γ increases beyond 1 towards the adiabatic limit, the dynamics exhibit coherent oscillations at the Rabi frequency, with energy transfer rates dictated by the decoherence time.

II. MODEL AND DYNAMICS

A. Donor-acceptor and cavity Hamiltonians

We write the total Hamiltonian, $H = H_{\mathcal{DA}} + H_{\rm cav}$, as a sum of the donor–acceptor vibronic Hamiltonian, $H_{\mathcal{DA}}$, and the contributions due to the cavity mode, $H_{\rm cav}$. The donor–acceptor vibronic Hamiltonian of the two QDs is derived from the model Hamiltonian developed by Jasrasaria and Rabani.[36,37] This model describes hot exciton relaxation in a single QD, where ultrafast relaxation dynamics are driven by multi–phonon channels.[38] Its generalization for a donor–acceptor system is given by

$$\begin{aligned} H_{\mathcal{DA}} = & \sum_{n\in\mathcal{D},\mathcal{A}} E_n \left|\psi_n\right\rangle \left\langle\psi_n\right| \\ & + \sum_{n\in\mathcal{D},m\in\mathcal{A}} J_{nm} \left(\left|\psi_n\right\rangle \left\langle\psi_m\right| + h.c.\right) \\ & + \sum_{\alpha\in\mathcal{D},\mathcal{A}} \hbar\omega_\alpha b_\alpha^\dagger b_\alpha + \sum_{n,m\in\mathcal{D},\mathcal{A}} V_{nm}^\alpha \left|\psi_n\right\rangle \left\langle\psi_m\right| q_\alpha . \end{aligned} \tag{2}$$

The first and second terms on the right hand side describe the manifold of donor and acceptor excitonic states and their couplings, respectively, and the remaining terms describe the lattice vibrations and the exciton–phonon couplings, approximated to lowest order in the phonons displacement, q_α. In the above, E_n is the energy of a singly excited state $|\psi_n\rangle$, with $n \in \mathcal{D}/\mathcal{A}$ and $\mathcal{D} = \{\mathcal{D}_1, \mathcal{D}_2, \cdots\}$, $\mathcal{A} = \{\mathcal{A}_1, \mathcal{A}_2, \cdots\}$. We use the notation $|\psi_{\mathcal{D}_1}\rangle$ to describe the donor in excitonic state $\mathcal{D}_1$ while the acceptor is in its ground state and vise versa for $|\psi_{\mathcal{A}_1}\rangle$. The excitonic energies and wave functions (E_n and $|\psi_n\rangle$) were obtained by ignoring the coupling between the donor and acceptor, using the semi–empirical pseudopotential methods combined with the Bethe–Salpeter equation (BSE).[37] The quasiparticle states near the top of the valence band and the bottom of the conduction band were generated for each QD using the filter diagonalization technique[39,40] with a real–space grid basis of $N_g \approx 2 \cdot 10^6$ and a grid spacing of $\approx 0.75 a_0$. A total of 80 electron (unoccupied) and 140 hole (occupied) states were generated to construct the Bethe–Salpeter Hamiltonian,[41] within the static screening approximation,[37] providing converged excitonic energies and transition dipole moments for the lowest 30 excitonic states that participate in the dynamics, for each QD.

The coupling between the donor in state $|\psi_{\mathcal{D}}\rangle$ and the acceptor in state $|\psi_{\mathcal{A}}\rangle$, $J_{\mathcal{DA}}$, was approximated to lowest order in the corresponding transition charge densities, with the dipole–dipole leading term given by:[20]

$$J_{\mathcal{DA}} = f_{\mathcal{D}} f_{\mathcal{A}} \frac{\left|\boldsymbol{\mu}_{\mathcal{D}}^{\rm ex}\right| \left|\boldsymbol{\mu}_{\mathcal{A}}^{\rm ex}\right|}{\epsilon_{\rm m} \left|R\right|^3} \kappa\left(\theta_{\mathcal{DA}}, \theta_{\mathcal{D}}, \theta_{\mathcal{A}}\right), \tag{3}$$

Here, $\boldsymbol{\mu}_{\mathcal{D}/\mathcal{A}}^{\rm ex} = \left\langle \psi_{\mathcal{D}/\mathcal{A}} \right| \hat{\boldsymbol{\mu}} \left| \psi_g \right\rangle$ is the transition dipole moment obtained from the pseudopotential model[37] and

$|\psi_g\rangle$ is the ground state. The local field factor in the above is given by $f_{\mathcal{D}/\mathcal{A}} = \frac{3}{2+\epsilon_{\mathcal{D}/\mathcal{A}}/\epsilon_{\mathrm{m}}} = \frac{3}{7}$ for[42] $\epsilon_{\mathcal{D}} = \epsilon_{\mathcal{A}} = 5$ and $\epsilon_{\mathrm{m}} = 1$, and $|\kappa(\theta_{\mathcal{DA}}, \theta_{\mathcal{D}}, \theta_{\mathcal{A}})| \leq 2$ is an angle dependent term which can be approximated by averaging over the angles, with the well-known results that $\sqrt{\langle\kappa^2\rangle} = \sqrt{\frac{2}{3}}$.[43] Alternatively, one can compute the angles $\theta_{\mathcal{DA}}$, $\theta_{\mathcal{D}}$, and $\theta_{\mathcal{A}}$, which depend on the relative orientation of the transition dipole moments.[44]

The donor and acceptor excitonic states also couple to the lattice vibrations with frequencies ω_α and modes $q_\alpha = \sqrt{\frac{\hbar}{2\omega_\alpha}}\left(b_\alpha^\dagger + b_\alpha\right)$, obtained by diagonalizing the dynamical matrix of the QD donor and acceptor using the Stilling–Weber force field parameterized for Cd, Se, S elements.[45] The exciton–phonon couplings were expanded to lowest order in the displacements, q_α, and the strength of coupling between exciton $\left|\psi_{\mathcal{D}/\mathcal{A}}\right\rangle$ to mode α was obtained from the pseudopotential Hamiltonian.[36] We assumed that the excitons are localized to the donor or the acceptor and thus, excitons only couple to the lattice modes of the donor or the acceptor. The coupling of excitons to the lattice vibrations is key in accounting for the reorganization and the relaxation of the system to thermal equilibrium.

The optical cavity was modeled by a single–mode Pauli–Fierz Hamiltonian within the dipole approximation and rotation wave approximation:[46,47]

$$\begin{aligned} H_{\mathrm{cav}} = \hbar\omega_c a^\dagger a + \sum_{n\in\mathcal{D},\mathcal{A}} \hbar g_n \left(a^\dagger \left|\psi_g\right\rangle\left\langle\psi_n\right| + h.c.\right) \\ + \frac{\hbar}{\omega_c}\sum_{n\in\mathcal{D},\mathcal{A}} g_n^2 \left|\psi_g\right\rangle\left\langle\psi_g\right| \\ + \frac{\hbar}{\omega_c}\sum_{n,m\in\mathcal{D},\mathcal{A}} g_n g_m \left(\left|\psi_n\right\rangle\left\langle\psi_m\right| + h.c.\right), \end{aligned} \tag{4}$$

where a ($a^\dagger$) is the annihilation (creation) operator of a photon with frequency ω_c, and $\hbar g_n$ is coupling strength between the cavity mode and an excitonic state $|\psi_n\rangle$ ($n \in \mathcal{D}/\mathcal{A}$). The cavity–exciton coupling strength is given by $g_n = \sqrt{\omega_c/\left(2\hbar\epsilon_{\mathrm{m}}\mathcal{V}\right)}\boldsymbol{\mu}_n^{\mathrm{ex}}\cdot\boldsymbol{k}$, where as before, $\boldsymbol{\mu}_n^{\mathrm{ex}}$ is the transition dipole moment from the ground state $|\psi_g\rangle$ to exciton $|\psi_n\rangle$ (obtained from the BSE calculation) and $\boldsymbol{k}$ is a unit vector of the polarization direction of the electromagnetic field. ϵ_{m} is the effective permittivity inside the cavity (medium) and $\mathcal{V}$ is the effective cavity quantization volume.

B. Polaritonic representation and polaron transformation

The total Hamiltonian can also be expressed using the polaritonic bases, $\{|\varphi_n\rangle = c_{ng}|\psi_g, 1\rangle + \sum_m c_{nm}^{\mathrm{ex}}|\psi_m, 0\rangle\}$, where $|\psi_g, 1\rangle$ and $|\psi_m, 0\rangle$ are the ground state with one photon or an excitonic state with zero photons, respectively. This representation simplifies the description of the dynamics within the Redfield approach described below, and is not limited by the weak donor-acceptor coupling strength (provided that the exciton-phonon couplings are small), as is the case for FRET between CdSe/CdS core-shell QDs. The coefficients c_{ng} and c_{nm}^{ex} were obtained by diagonalizing the system Hamiltonian, defined by (we assume that the ground state energy, $E_g = 0$):

$$\begin{aligned} H_{\mathrm{S}} = H_{\mathrm{cav}} + \sum_{n\in\mathcal{D},\mathcal{A}} E_n \left|\psi_n\right\rangle\left\langle\psi_n\right| \\ + \sum_{n\in\mathcal{D},m\in\mathcal{A}} J_{nm}\left(\left|\psi_n\right\rangle\left\langle\psi_m\right| + h.c.\right). \end{aligned} \tag{5}$$

In addition, to properly describe dephasing and relaxation and to account for ultrafast multi–phonon relaxation channels, we performed a small polaron transformation as detailed in Ref. 38,47. The total transformed Hamiltonian $\mathcal{H}$ in the polaritonic basis is given

$$\begin{aligned} \mathcal{H} = \overbrace{\sum_n \left(\tilde{E}_n - \lambda_n\right)\left|\varphi_n\right\rangle\left\langle\varphi_n\right|}^{\mathcal{H}_{\mathrm{S}}} \\ + \overbrace{\sum_\alpha \hbar\omega_\alpha b_\alpha^\dagger b_\alpha}^{\mathcal{H}_{\mathrm{B}}} + \overbrace{\sum_{n\neq m} W_{nm}\left|\varphi_n\right\rangle\left\langle\varphi_m\right|}^{\mathcal{H}_{\mathrm{I}}}. \end{aligned} \tag{6}$$

In the above, the dressed coupling is given by

$$\begin{aligned} W_{nm} = \exp\left(-\frac{i}{\hbar}\sum_\gamma \frac{p_\gamma \tilde{V}_{nn}^\gamma}{\omega_\gamma^2}\right)\times \\ \times\left[\sum_\alpha \tilde{V}_{nm}^\alpha q_\alpha\right]\exp\left(+\frac{i}{\hbar}\sum_\xi \frac{p_\xi \tilde{V}_{mm}^\xi}{\omega_\xi^2}\right). \end{aligned} \tag{7}$$

As evident, the dressed coupling depends exponentially on the momenta of all phonon modes, enabling multi–phonon relaxation, even at the lowest order perturbation in $\mathcal{H}_{\mathrm{I}}$. In the above equations, $\tilde{E}_n$ and $\lambda_n = \frac{1}{2}\sum_\alpha\left(\tilde{V}_{nn}^\alpha\right)^2/\omega_\alpha^2$ are the energy and reorganization energy (polaron shift) of polaritonic state $|\varphi_n\rangle$, respectively. The reorganization energy depends on $\tilde{V}_{nm}^\alpha$, the coupling matrix element between two polaritonic states $|\varphi_n\rangle$ and $|\varphi_m\rangle$ and phonon mode α. $\tilde{V}_{nm}^\alpha$ was obtained by applying the unitary transformation U that diagonalizes H_{S} to $\tilde{V}^\alpha = U^\dagger V^\alpha U$, for each mode α. p_α is the momentum operator of vibrational mode α.

C. Dynamics

In this work, we leverage on the fact that the rescaled coupling between polaritons and phonon, $\mathcal{H}_{\mathrm{I}}$ (Eq. (6)), can be treated perturbatively. Thus, to generate the dynamics within the Hilbert space of polaritons, we adopt the Redfield equations instead of using more advanced

methods suitable for strong coupling.[48] The equation of motion for the reduced density matrix, $\sigma(t)$, representing the polaritonic subspace can then be written as:[49]

$$\begin{aligned}\frac{d\sigma(t)}{dt} &= -\frac{i}{\hbar}\left[\mathcal{H}_{\rm S} + \langle\mathcal{H}_{\rm I}\rangle_{\rm B}, \sigma(t)\right] \\ &-\frac{1}{\hbar^2}\sum_{nm,kl}\int_0^t d\tau\left\{C_{nm,kl}(\tau)\left[\left(\mathcal{H}_{\rm S}^{\rm I}\right)_{nm}, e^{-i/\hbar\mathcal{H}_{\rm S}\tau}\left(\mathcal{H}_{\rm S}^{\rm I}\right)_{kl}\sigma(t-\tau)\,e^{i/\hbar\mathcal{H}_{\rm S}\tau}\right]\right. \\ &\left. - C^*_{nm,kl}(\tau)\left[\left(\mathcal{H}_{\rm S}^{\rm I}\right)_{nm}, e^{-i/\hbar\mathcal{H}_{\rm S}\tau}\sigma(t-\tau)\left(\mathcal{H}_{\rm S}^{\rm I}\right)_{kl}e^{i/\hbar\mathcal{H}_{\rm S}\tau}\right]\right\}, \end{aligned} \tag{8}$$

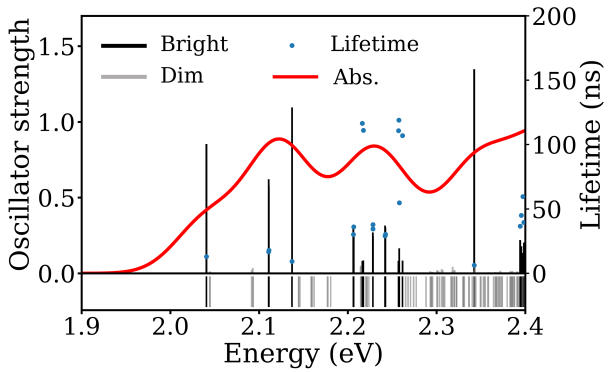

Figure 2. The calculated linear absorption spectrum for CdSe/CdS core–shell NCs, with a CdSe core diameter of 3 nm and 2 monolayers of CdS shell. The vertical lines in upper subplot indicate the magnitude of the oscillator strength of the transition from the ground state to that excitonic state. The continuous absorption spectra (red curve) was obtained by broadening the individual transitions with a variance of 35 meV Gaussian function. The blue dots indicate the radiative lifetime of each excitonic state given by Eq. (10) below. The lower subplot in this figure shows the density of excitonic states.

where the polariton-phonon coupling is expressed as $\mathcal{H}_{\rm I} = \sum_{nm} W_{nm}\left(\mathcal{H}_{\rm S}^{\rm I}\right)_{nm}$ with $\left(\mathcal{H}_{\rm S}^{\rm I}\right)_{nm} = (1-\delta_{nm})\,|\varphi_n\rangle\langle\varphi_m|$. In the above equation, $\langle\cdots\rangle_{\rm B}$ denotes an equilibrium thermal average over the so called "bath" degrees of freedom. The bath correlation function appearing above given by:

$$C_{nm,kl}(t) = \langle W_{nm}(t)\,W_{kl}(0)\rangle_{\rm B} - \langle W_{nm}\rangle_{\rm B}\langle W_{kl}\rangle_{\rm B}, \tag{9}$$

with $W_{nm}(t) = e^{i/\hbar\mathcal{H}_{\rm B}t}W_{nm}e^{-i/\hbar\mathcal{H}_{\rm B}t}$. These thermal averages and thermal correlation functions were computed analytically for the above Hamiltonian as further described in the supporting information.

III. EXCITON ENERGY TRANSFER BETWEEN QDS

In this section, we examine the excitonic structure of a typical 3 nm CdSe core with a 2-monolayer CdS shell and compare the predicted radiative lifetimes to experimental data. Additionally, we demonstrate that the Redfield approach, which treats the dressed exciton–phonon coupling perturbatively but includes all orders of the hybridization J_{nm}, aligns well with Förster theory in the absence of a cavity. The main purpose of this section is to provide further validation for the approach developed herein and in particular, for the calculated oscillator strengths and vibronic couplings, essential to accurately describe the energy transfer mechanisms and rates.

Fig. 2 presents the calculated absorption spectrum of a typical 3 nm CdSe core with a 2-monolayer CdS shell, alongside the density of excitonic states. The absorption onset is marked by several distinct "bright" excitonic transitions, highlighted by vertical lines representing the oscillator strength. As excitonic energy increases, the

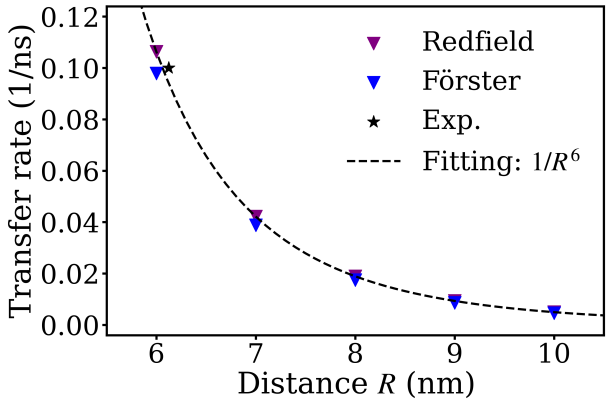

Figure 3. Excitation energy transfer rates between two QDS, one with a 3.9nm CdSe core and 3 monolayers CdS shell, the other with a 3.9nm CdSe core 4 monolayers CdS shell, as a function of center-to-center distances between QDs, at 300K. The purple triangles represent the rates obtained from Eq. (8) (labeled as "Redfield"); the blue triangles depict the rates calculated directly from Fermi's Golden Rule (Förster theory) as in Eq. (1) (labeled as "Förster"). The black star is an experimental measurement between two CdSe QDs of different sizes, 3.85nm and 6.2nm in diameter, respectively.[50] The dash line depicts a R^{-6} relationship and is a guide to the eye.

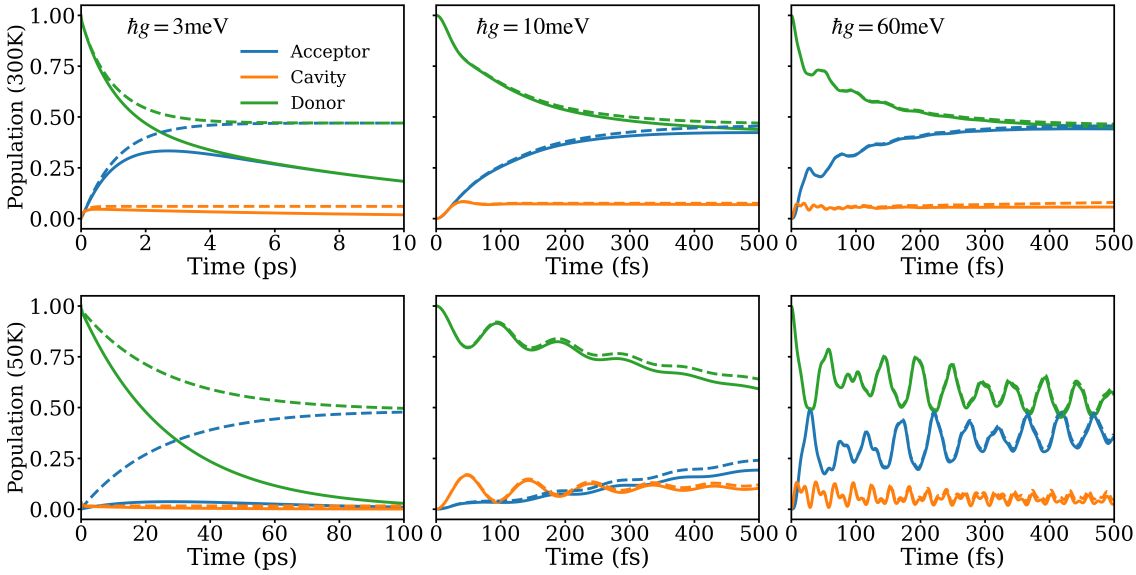

Figure 4. Population dynamics for different light–matter interaction strengths and different temperatures. The dashed and solid lines represent results from a lossy and ideal cavity, respectively. The donor–acceptor distance was fixed at 6 nm. Three different QD-cavity couplings were considered, 3 meV, 10 meV, and 60 meV, corresponding to effective coupling of 0.5 meV, 4 meV, and 40 meV, respectively.

density of excitons rises rapidly, with the appearance of many "dim" transitions arising from the high density of holes.[38,51] The bright excitons play a crucial role in the energy transfer between the donor and acceptor, whereas the dim excitons are essential to account for dephasing and relaxation. To accurately describe both energy transfer dynamics and the relaxation to equilibrium, we include the 30 lowest excitonic states for each QD, namely 30 states for the donor and the acceptor. Fig. 2 also shows the calculated radiative lifetime for each excitonic state, obtained from

$$\tau_n^{\mathrm{ex}} = \frac{3c^3}{4E_n^3 \left|\boldsymbol{\mu}_n^{\mathrm{ex}}\right|^2}. \tag{10}$$

The thermal average radiative lifetime, $\tau^{\mathrm{ex}} = \sum_n P_n \tau_n^{\mathrm{ex}}$ (P_n is the Boltzmann population of exciton $|\psi_n\rangle$), is found to be 24 ns, in very good agreement with experimental measurements, ranging between $21 - 28$ ns.[52–55]

In Fig. 3, we plot the calculated energy transfer rates as a function of the distance between the two QDs in the absence of a cavity. This is used to assess the accuracy of the Redfield approach in describing the energy transfer dynamics in the FRET limit, which can be compared to Förster perturbation theory as well as experimental values. The Redfield rates were obtained by fitting the calculated longtime population dynamics, $\rho_{\mathcal{D}/\mathcal{A}}(t) = \sum_{n\in\mathcal{D}/\mathcal{A}} \sigma_{nn}(t)$, to an exponential decay:

$$\rho_{\mathcal{D}}(t) = (1 - P_{\mathcal{D}}^{\mathrm{eq}}) \exp\left[-k_{\mathrm{ET}} t\right] + P_{\mathcal{D}}^{\mathrm{eq}} \tag{11}$$

where $P_{\mathcal{D}}^{\mathrm{eq}}$ is the donor total exciton population at equilibrium and k_{ET} is the energy transition rate. For implementing Förster theory (Eq. (1)), we have convoluted the absorption transition with a Gaussian broadening function, with a width (≈ 60 meV) taken from the calculated photoluminescence spectrum.[56] The energy transfer rates calculated by both methods agree quite well with each other (note that the Förster theory rate depends on the choice of the broadening) and both recover the R^{-6} distance dependence, as expected. The calculated results are within a reasonable range compared to experimental measurements,[50,57] also shown in Fig. 3.

IV. POLARITONIC ENERGY TRANSFER BETWEEN QDS

We now turn to discuss the role of the cavity mode in the exciton transfer dynamics. We consider the transfer between two CdSe/CdS core-shell QDs with 3 nm core size and 2 layers of CdS shell and a core-to-core distance of 6 nm. The photon energy was set to $\hbar\omega_c = 2.06$ eV, slightly above the absorption onset of the QDs and the orientation of the QDs was fixed with the dipole moment parallel to the cavity polarization vector. The cavity coupling strength to the lowest donor excited state $\hbar g_{\mathcal{D}_1} \equiv \hbar g$ is used as a measure of the QD-cavity coupling strength. We considered two scenarios, an ideal cavity without energy loss and a more realistic cavity with a photon escape time of[58] $\tau_{\mathrm{cav}} = 0.5$ ps. We prepare the system in an initial thermal population of the excitonic states on the donor and a canonical distribution of all phonon modes.

Fig. 4 shows representative population dynamics for an ideal cavity (dashed lines) and a "lossy" cavity (solid lines) at two different temperatures and varying cavity-QD coupling values. The behavior of the donor and ac-

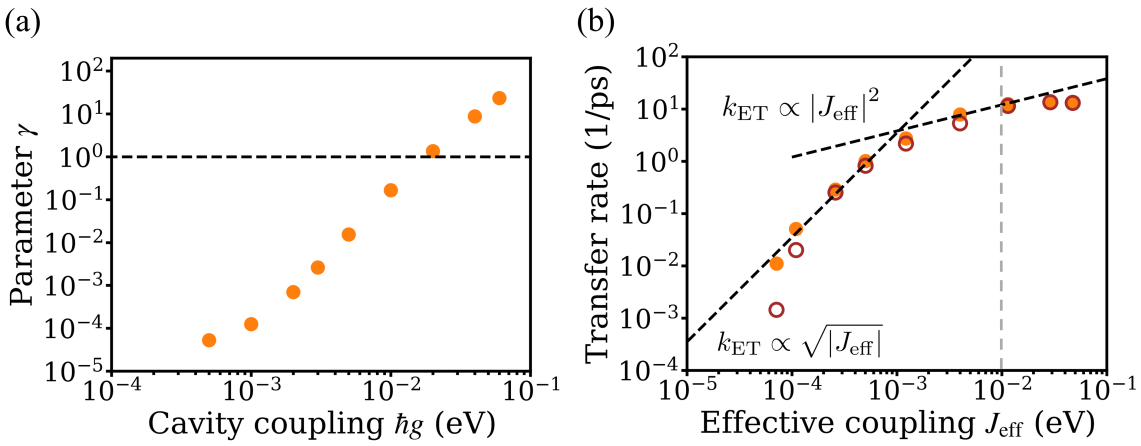

Figure 5. (a) Plot of the nonadiabatic parameter γ versus the QD-cavity coupling strength $\hbar g$ at 300K. The dashed line shows $\gamma = 1$. (b)Energy transfer rate k_{ET} as a function of effective coupling J_{eff} for ideal cavity (orange dots) and lossy cavity (red hollow circles) at 300K. The black dashed lines show a quadratic and square root dependence and the gray dashed line corresponds to an effective coupling for $\gamma = 1$.

ceptor populations is qualitatively similar for the ideal and lossy cavities on timescales relevant to energy transfer. At low QD-cavity couplings ($\hbar g = 1$ meV), the donor population dynamics exhibit a single exponential decay with a rate approximated by Eq. (11). The coupling of both QDs to the same cavity mode results in an effective direct coupling between them (see supporting information), estimated by tunneling splitting $J_{eff} = \frac{1}{2}\left(\tilde{E}_{LP+1} - \tilde{E}_{LP}\right)$,[59–61] where $\tilde{E}_{LP}$ and $\tilde{E}_{LP+1}$ are the two lowest polaritonic energies obtained by diagonalizing H_S, as described above. This effective coupling is much larger than the direct dipole-dipole coupling given by Eq. (3). As $\hbar g$ increases above 40 meV, the population dynamics display pronounced oscillations with a frequency approximately equal to $2J_{eff}$. In this case, the exciton transfer rate is governed by decoherence time, especially at lower temperatures. A similar transition from incoherent to coherent dynamics has recently been reported for electron transfer between fused NC QDs.[62]

To better understand the transition from the overdamped to the coherent regime and make connections with previous works, we define a nonadiabatic parameter γ, given by:[63,64]

$$\gamma = \frac{|J_{eff}|^2}{\hbar\omega_{nu}}\sqrt{\frac{\pi^3}{(\lambda_{\mathcal{D}} + \lambda_{\mathcal{A}})\, k_B T}}, \tag{12}$$

where $\omega_{nu} = \sqrt{\frac{\sum_\alpha \omega_\alpha^2 \lambda_\alpha}{\sum_\alpha \lambda_\alpha}}$ is the average phonon frequency weighted by the reorganization energy for each phonon mode. The terms $\lambda_{\mathcal{D}}$ and $\lambda_{\mathcal{A}}$ represent the average reorganization energies for the donor and acceptor, respectively, defined as $\lambda_{\mathcal{D}/\mathcal{A}} = \sum_{n\in\mathcal{D}/\mathcal{A}} P_n \lambda_n$, where P_n is the Boltzmann population distribution of exciton $|\psi_n\rangle$ and, as before, $\lambda_n = \frac{1}{2}\sum_\alpha \left(\tilde{V}_{nn}^\alpha\right)^2 / \omega_\alpha^2$. In Fig. 5(a) we plot the nonadiabatic parameter γ as a function of the QD-cavity coupling strength $\hbar g$. For small coupling to the cavity mode, $\gamma \ll 1$ and the system is in the nonadiabatic regime, where the dynamics are characterized by an exponential decay of populations. As the coupling to the cavity mode increases, γ also increases due to the increase in the effective coupling between the two QDs. This parameter reaches and surpasses $\gamma = 1$ when $\hbar g = 40$ meV, marking the transition to an adiabatic regime. In this regime, the effective coupling strength between the QDs becomes significantly larger than the couplings of the donor and acceptor polaritonic states to phonons, leading to more pronounced and sustained coherent dynamics.

In Fig. 5(b), we present the exciton transfer rate as a function of the effective coupling for both ideal and lossy cavities. For small value of J_{eff}, the transfer rate scales with J_{eff}^2, consistent with Fermi's golden rule. As J_{eff} increases, the system transitions to the adiabatic regime, and the transfer rate which is determined by decoherence times exhibits a more moderate dependence, fitting to a $\sqrt{J_{eff}}$ relationship. The gray dashed line in the figure marks the crossover coupling point, where the adiabatic parameter $\gamma = 1$. In the lossy cavity, the energy transfer rate is inherently slower when compared to an ideal, lossless cavity. However, as the coupling to the cavity mode is increased, this discrepancy becomes less significant. This is because the rate of energy transfer accelerates, eventually becoming so rapid that it surpasses the cavity's inherent loss rate. As a result, the effects of the cavity's losses are effectively mitigated, rendering them negligible in the context of the swift energy transfer times that are achieved.

V. CONCLUSION

In this study, we investigated the dynamics of exciton energy transfer between two nanocrystal quantum dots positioned within an optical microcavity. We delved into this intricate phenomenon, examining how the cavity photon mode influences the energy transfer process between the quantum dots, essentially serving as a conduit. To achieve this, we developed a model Hamiltonian, parameterized by atomistic calculations of the excitonic level structure, phonon, exciton-phonon couplings, and transition dipole moments of the semiconductor NCs within the microcavity. To describe the dynamics comprehensively, we utilized a quantum master equation and approximated its kernel to second order in the exciton-phonon coupling (Redfield with memory), while also performing a small polaron transformation to account for multiphonon relaxation channels.

Our investigation revealed that by fine-tuning the coupling strength between the cavity photon mode and the NCs, we can effectively modulate the interaction between the donor and acceptor. Particularly noteworthy is the identification of a critical transition from a nonadiabatic to an adiabatic process, wherein the exciton energy transition rate is accelerated and governed by decoherence times. This transition holds significant implications for the controllability and efficiency of energy transfer processes at the nanoscale. Overall, our findings lay the groundwork for the design of innovative energy transfer systems and nanophotonic devices, promising enhanced functionality and performance in various applications.

SUPPLEMENTARY MATERIAL

The supplementary material comprises nanocrystal configurations, simplification of correlation function $\langle W_{nm}(t) W_{kl}(0)\rangle_{\mathrm{B}}$, and derivation of the effective coupling for a 3-level system.

ACKNOWLEDGMENTS

This work was supported by the U.S. Department of Energy, Office of Science, Office of Basic Energy Sciences, Materials Sciences and Engineering Division, under Contract No. DE461AC02-05-CH11231 within the Fundamentals of Semiconductor Nanowire Program (KCPY23). Computational resources were provided in part by the National Energy Research Scientific Computing Center (NERSC), a U.S. Department of Energy Office of Science User Facility operated under contract no. DEAC02-05CH11231.

AUTHOR DECLARATIONS

Conflict of Interest Statement

The authors have no conflicts to disclose.

Author Contributions

Kaiyue Peng: Data curation (lead); Formal analysis (lead); Software (lead), Methodology (equal); Project administration (equal); Conceptualization (equal); Validation (lead); Writing – original draft (equal). Eran Rabani: Funding Acquisition (lead), Resources (lead), Supervision (lead), Writing/Review and Editing (lead), Methodology (equal), Project Administration (equal), Conceptualization (equal); Writing – original draft (equal).

DATA AVAILABILITY STATEMENT

The data that support the findings of this study are available from the corresponding authors upon reasonable request.

REFERENCES

[1]S. Choi, H. Jin, J. Bang, and S. Kim, The Journal of Physical Chemistry Letters **3**, 3442 (2012).
[2]L. Zhao, T. Ming, L. Shao, H. Chen, and J. Wang, J. Phys. Chem. C **116**, 8287 (2012).
[3]J. Almutlaq, Y. Liu, W. J. Mir, R. P. Sabatini, D. Englund, O. M. Bakr, and E. H. Sargent, Nature Nanotechnology , 1 (2024).
[4]A. P. Alivisatos, The Journal of Physical Chemistry **100**, 13226 (1996).
[5]A. L. Efros and M. Rosen, Annual Review of Materials Science **30**, 475 (2000).
[6]D. E. Gomez, M. Califano, and P. Mulvaney, Physical Chemistry Chemical Physics **8**, 4989 (2006).
[7]V. I. Klimov, Annu. Rev. Phys. Chem. **58**, 635 (2007).
[8]M. S. Kodaimati, S. Lian, G. C. Schatz, and E. A. Weiss, Proceedings of the National Academy of Sciences **115**, 8290 (2018).
[9]P. Roy, G. Devatha, S. Roy, A. Rao, and P. P. Pillai, J. Phys. Chem. Lett. **11**, 5354 (2020).
[10]M. S. Kodaimati, C. Wang, C. Chapman, G. C. Schatz, and E. A. Weiss, ACS nano **11**, 5041 (2017).
[11]G. D. Scholes, X. J. Jordanides, and G. R. Fleming, J. Phys. Chem. B **105**, 1640 (2001).
[12]A. Barth, O. Opanasyuk, T.-O. Peulen, S. Felekyan, S. Kalinin, H. Sanabria, and C. A. Seidel, The Journal of Chemical Physics **156** (2022).
[13]J. Guo, X. Qiu, C. Mingoes, J. R. Deschamps, K. Susumu, I. L. Medintz, and N. Hildebrandt, ACS nano **13**, 505 (2018).
[14]E. A. Jares-Erijman and T. M. Jovin, Nature biotechnology **21**, 1387 (2003).
[15]J.-Y. Kim, C. Kim, and N. K. Lee, Nature communications **6**, 6992 (2015).
[16]C. E. Rowland, C. W. Brown, I. L. Medintz, and J. B. Delehanty, Methods and applications in fluorescence **3**, 042006 (2015).
[17]Y. Sun, H. Wallrabe, S.-A. Seo, and A. Periasamy, Chemphyschem **12**, 462 (2011).

[18]K. Zhong, H. L. Nguyen, T. N. Do, H.-S. Tan, J. Knoester, and T. L. Jansen, The Journal of Chemical Physics **158** (2023).
[19]R. M. Clegg, in *Reviews in fluorescence 2006* (Springer, 2006) pp. 1–45.
[20]R. Baer and E. Rabani, J. Chem. Phys. **128** (2008).
[21]M. Lunz, A. L. Bradley, V. A. Gerard, S. J. Byrne, Y. K. Gun'Ko, V. Lesnyak, and N. Gaponik, Physical Review B **83**, 115423 (2011).
[22]A. Loiudice, S. Saris, and R. Buonsanti, J. Phys. Chem. Lett. **11**, 3430 (2020).
[23]M. Cardoso Dos Santos, W. R. Algar, I. L. Medintz, and N. Hildebrandt, TrAC, Trends Anal. Chem. **125**, 115819 (2020).
[24]A. O. Govorov, J. Lee, and N. A. Kotov, Phys. Rev. B **76**, 125308 (2007).
[25]J. Schachenmayer, C. Genes, E. Tignone, and G. Pupillo, Phys. Rev. Lett. **114**, 196403 (2015).
[26]M. Wang, M. Hertzog, and K. Börjesson, Nat. Commun. **12**, 1874 (2021).
[27]S. N. Chowdhury, P. Zhang, and D. N. Beratan, J. Phys. Chem. Lett. **13**, 9822 (2022).
[28]B. Albinsson and J. Mårtensson, Physical Chemistry Chemical Physics **12**, 7338 (2010).
[29]D. Xu, A. Mandal, J. M. Baxter, S.-W. Cheng, I. Lee, H. Su, S. Liu, D. R. Reichman, and M. Delor, Nature Communications **14**, 3881 (2023).
[30]J. Feist and F. J. Garcia-Vidal, Phys. Rev. Lett. **114**, 196402 (2015).
[31]A. Kimura, J. Chem. Phys. **130** (2009).
[32]B. M. Weight, T. D. Krauss, and P. Huo, The Journal of Physical Chemistry Letters **14**, 5901 (2023).
[33]L. P. Lindoy, A. Mandal, and D. R. Reichman, Nature Communications **14**, 2733 (2023).
[34]B. Xiang, R. F. Ribeiro, M. Du, L. Chen, Z. Yang, J. Wang, J. Yuen-Zhou, and W. Xiong, Science **368**, 665 (2020).
[35]J. P. Philbin and E. Rabani, Nano Lett. **18**, 7889 (2018).
[36]D. Jasrasaria and E. Rabani, Nano Lett. **21**, 8741 (2021).
[37]D. Jasrasaria, D. Weinberg, J. P. Philbin, and E. Rabani, J. Chem. Phys. **157**, 020901 (2022).
[38]D. Jasrasaria and E. Rabani, Npj Comput. Mater. **9**, 1 (2023).
[39]M. R. Wall and D. Neuhauser, J. Chem. Phys. **102**, 8011 (1995).
[40]S. Toledo and E. Rabani, J. Comput. Phys. **180**, 256 (2002).
[41]M. Rohlfing and S. G. Louie, Phys. Rev. B **62**, 4927 (2000).
[42]L.-W. Wang and A. Zunger, Phys. Rev. B **53**, 9579 (1996).
[43]S. Latt, H. Cheung, and E. Blout, J. Am. Chem. Soc. **87**, 995 (1965).
[44]I. Fedchenia and P.-O. Westlund, Physical Review E **50**, 555 (1994).
[45]X. Zhou, D. Ward, J. Martin, F. Van Swol, J. Cruz-Campa, and D. Zubia, Phys. Rev. B **88**, 085309 (2013).
[46]A. Mandal, T. D. Krauss, and P. Huo, J. Phys. Chem. B **124**, 6321 (2020).
[47]K. Peng and E. Rabani, Nano Lett. **23**, 10587 (2023).
[48]J. B. Pérez-Sánchez, A. Koner, N. P. Stern, and J. Yuen-Zhou, Proceedings of the National Academy of Sciences **120**, e2219223120 (2023).
[49]A. Nitzan, *Chemical dynamics in condensed phases: relaxation, transfer and reactions in condensed molecular systems* (Oxford university press, 2006).
[50]C. Kagan, C. Murray, M. Nirmal, and M. Bawendi, Physical Review Letters **76**, 1517 (1996).
[51]P. J. Brosseau, J. J. Geuchies, D. Jasrasaria, A. J. Houtepen, E. Rabani, and P. Kambhampati, Commun. Phys. **6**, 48 (2023).
[52]F. T. Rabouw, M. Kamp, R. J. van Dijk-Moes, D. R. Gamelin, A. F. Koenderink, A. Meijerink, and D. Vanmaekelbergh, Nano Lett. **15**, 7718 (2015).
[53]W. K. Bae, L. A. Padilha, Y.-S. Park, H. McDaniel, I. Robel, J. M. Pietryga, and V. I. Klimov, ACS nano **7**, 3411 (2013).
[54]W. K. Bae, Y.-S. Park, J. Lim, D. Lee, L. A. Padilha, H. McDaniel, I. Robel, C. Lee, J. M. Pietryga, and V. I. Klimov, Nat. Commun. **4**, 2661 (2013).
[55]S. Crooker, J. Hollingsworth, S. Tretiak, and V. I. Klimov, Phys. Rev. Lett. **89**, 186802 (2002).
[56]K. Lin, D. Jasrasaria, J. J. Yoo, M. Bawendi, H. Utzat, and E. Rabani, J. Phys. Chem. Lett. **14**, 7241 (2023).
[57]Z. Lingley, S. Lu, and A. Madhukar, Nano letters **11**, 2887 (2011).
[58]B. le Feber, F. Prins, E. De Leo, F. T. Rabouw, and D. J. Norris, Nano Lett. **18**, 1028 (2018).
[59]D. Davis, M. C. Toroker, S. Speiser, and U. Peskin, Chem. Phys. **358**, 45 (2009).
[60]S. S. Skourtis, G. Archontis, and Q. Xie, J. Chem. Phys. **115**, 9444 (2001).
[61]S. Priyadarshy, S. S. Skourtis, S. M. Risser, and D. N. Beratan, J. Chem. Phys. **104**, 9473 (1996).
[62]B. Hou, M. Thoss, U. Banin, and E. Rabani, Nat. Commun. **14**, 3073 (2023).
[63]M. D. Newton and N. Sutin, Annu. Rev. Phys. Chem. **35**, 437 (1984).
[64]V. Balzani, P. Piotrowiak, M. Rodgers, J. Mattay, D. Astruc, *et al.*, *Electron transfer in chemistry*, Vol. 1 (Wiley-VCh Weinheim, 2001).